

Is the cold spot responsible for the CMB North-South asymmetry?

Armando Bernui^{1,2}

¹*Divisão de Astrofísica, Instituto Nacional de Pesquisas Espaciais
Av. dos Astronautas 1758, 12227-010, São José dos Campos, SP, Brazil*

²*Centro Brasileiro de Pesquisas Físicas,
Rua Dr. Xavier Sigaud 150, 22290-180, Rio de Janeiro, RJ, Brazil*

Several intriguing phenomena, unlikely within the standard inflationary cosmology, were reported in the cosmic microwave background (CMB) data from WMAP and appear to be uncorrelated. Two of these phenomena, termed CMB anomalies, are representative of their disparate nature: the North-South asymmetry in the CMB angular-correlation strength, inconsistent with an isotropic universe, and the cold spot, producing a significant deviation from Gaussianity. We find a correlation between them, at medium angular scales ($\ell = 11 - 20$): we show that a successive diminution of the cold spot (absolute-value) temperature implies a monotonic decrease of the North-South asymmetry power, and moreover we find that the cold spot supplies 60% of such power.

PACS numbers: 98.70.Vc, 98.80.Es

I. INTRODUCTION

Successive data releases from the Wilkinson Microwave Anisotropy Probe (WMAP) [1] have confirmed the validity of the standard inflationary cosmological model Λ CDM, which asserts that the observed cosmic microwave background (CMB) temperature fluctuations are a stochastic realization of an isotropic Gaussian random field on the celestial sphere. This means that the CMB sky should exhibit statistical isotropy and statistical Gaussianity attributes.

Close scrutiny of the CMB WMAP maps have revealed highly significant departures both from statistical isotropy and from Gaussianity at large and medium angular scales. Evidences of an anomalous power asymmetry of the CMB angular correlations between the northern and southern ecliptic hemispheres (termed the NS-asymmetry) indicate that the CMB temperature field is inconsistent with the statistical isotropy expected in the model [2]. Another intriguing detection concerns an anomalously cold and large spot (termed the cold spot), centered at $(l, b) \simeq (209^\circ, -57^\circ)$ in galactic coordinates, which causes a significant deviation from Gaussianity [3].

Many attempts have been made to explain these phenomena, termed CMB anomalies, in particular, within the standard inflationary Λ CDM scenario where they are unlikely at $\lesssim 1\%$ of probability. Hypotheses like instrumental noise, systematic errors (e.g., in the mapmaking process), the inhomogeneous exposure function of the probe, incomplete sky-data (due to the cut-sky mask), unmodeled foreground emissions [4], and physical mechanisms that break statistical isotropy (e.g., during the epoch of inflation or during the decoupling era, as for instance, primordial magnetic fields) [5], have been extensively investigated. Unfortunately, none of them seems to explain satisfactorily the reported CMB anomalies.

Another way to comprehend these phenomena is to look for possible correlations between them, or establish their absence. Clearly, finding a cause-effect relationship between CMB anomalies would simplify the search for

their origin. For instance, [6] proved the absence of correlation between the alignment of low order multipoles and the observed lack of CMB angular correlations on scales $> 60^\circ$. On the other hand, [7] found that the alignment of the CMB quadrupole and octopole is not responsible for the anomalous NS-asymmetry at large angles. Likewise, using needlets [8] detected anomalous spots in the needlets' coefficients map. However, it seems possible that one of such spots could be caused by the CMB cold spot. In such a case the hemispherical asymmetry found in the needlets' power spectrum [8] could be related to the CMB cold spot.

In this work we show that the cold spot is responsible for 60% of the NS-asymmetry strength in WMAP maps at medium angular scales (i.e., maps with multipoles $\ell = 11 - 20$). Firstly, we prove that the NS-asymmetry is present at 94%–98% C.L. in these maps. Then we show that gradually reducing the cold-spot temperature (turning it less cold) turns the NS-asymmetry effect less and less statistically significant. When the cold spot is suppressed the statistical significance of the NS-asymmetry phenomenon goes to the level found in the average from statistically-isotropic Gaussian CMB maps.

II. WMAP DATA

Substantial efforts done by the WMAP science team to minimize foregrounds and to limit systematic errors resulted in the five-year foreground-reduced single-frequency Q, V, and W band-maps [1]. Our aim is to investigate the angular distribution and statistical features of the CMB temperature field in these Q, V, and W maps at medium angular scales, that is, maps with multipole components $\ell = 11 - 20$. To obtain such data we first perform the multipolar decomposition of the original maps, applying the recommended KQ75 mask [1], by using the ANAFast code [9]. After that, we select the multipole components $11 \leq \ell \leq 20$ and generate the corresponding CMB map with the SYNFAST code [9].

In the top panel of Fig. 1 we exhibit the V map containing the multipoles $\ell = 11 - 20$. The Q and W maps are fully similar to this V map, as corroborated by Pearson's coefficient p_{AB} that measures the pixel-to-pixel correlation between A and B maps: $p_{VQ} = 0.9985$, $p_{VW} = 0.9982$, and $p_{QW} = 0.9976$. In this V map one clearly observes a large blue spot in the lower right corner: this is the cold spot with radius about 8° and centered at $(l, b) \simeq (209^\circ, -57^\circ)$.

A statistical analysis (outside the KQ75 region) reveals that the skewness of the Q, V, and W maps is -0.124, -0.125, and -0.127, respectively, indicating that the temperature distribution is skewed to the left with a longer tail for negative CMB values. For comparison, notice that Monte Carlos Gaussian maps (described in detail below) have skewness mean: 0.0012 ± 0.0853 . Notice also that in less than 5% of the Monte Carlos Gaussian maps one finds skewness values larger than those values found in WMAP data and this fact just represent the ergodicity of the data.

For completeness, we shall analyze the temperature distribution in original and modified WMAP maps, termed X-cases, in which the cold-spot temperature is reduced. Consider the set of n cold-spot pixels, that is, those pixels of the WMAP map belonging to the cap centered at $(209^\circ, -57^\circ)$ and within 8° of radius. Let $\{T_i^{cs}; i = 1, \dots, n\}$ be the set of cold spot pixels' temperatures of a WMAP map: the X-case corresponds to reducing these temperatures to X% of the original ones, while leaving all the other map pixels intact. For instance, X=90 means that the cold-spot pixels' temperatures were reduced to the values $0.9 \times T_i^{cs}$. Clearly, X=100 or 100%-case refers to the original WMAP map. For X=0 we replace the cold-spot temperature by the mean temperature of the WMAP map outside the KQ75 region, that is, $\sim -10^{-5}$ mK.

We exhibit the temperature distribution for the V map in the bottom panel of Fig. 1, although in an atypical format in order to enhance possible deviations from a Gaussian distribution. In the horizontal axis we plot the square of the temperatures T^2 and in the vertical axis we have the number of pixels in logarithmic scale. In this picture, a Gaussian curve $= (1/\sigma_G \sqrt{2\pi}) e^{-\frac{1}{2}(T^2/\sigma_G^2)}$ is transformed into a straight line. We plotted four data sets: (i) The straight (blue) line is the expected Gaussian distribution, for positive and negative CMB temperature fluctuations because a Gaussian is symmetric with respect to zero, with variance $\sigma_G^2 = 4.65 \times 10^{-4}$ mK². (ii) The histogram (red) curve corresponds to the negative temperatures of the V map. (iii) The dashed (violet) line corresponds to the positive temperatures of the V map. (iv) The triangles represent the negative temperatures of the case X=70 for the V map. As predicted by the skewness value, the (red) histogram curve reveals a non-linear tail due to pixels with anomalously large negative temperatures $T \lesssim -0.07$ mK (or $T^2 \gtrsim 0.0045$ mK²), and we want to know if the cold spot [3] is related to this effect. Instead of masking the cold spot in a

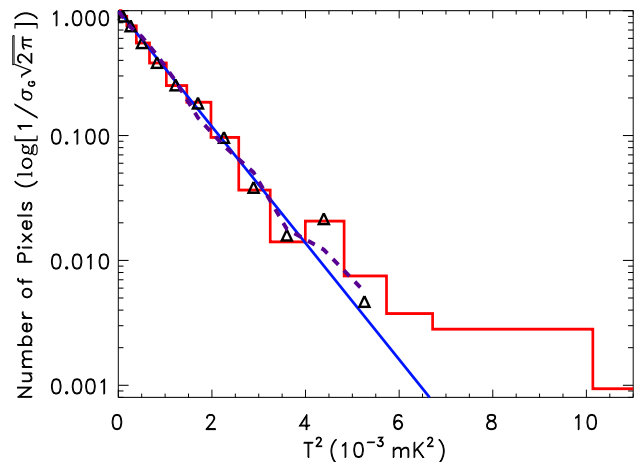
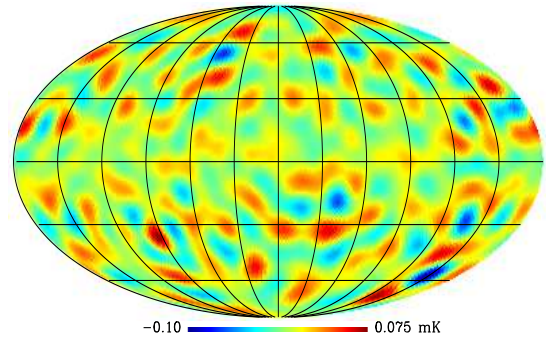


FIG. 1: Top: This is the V map with multipole components $\ell = 11 - 20$, obtained using the KQ75 mask. Bottom: This plot shows the temperature distribution of this V map, considering data outside the KQ75 region, where: (i) the straight (blue) line is the expected Gaussian distribution with variance $\sigma_G^2 = 4.65 \times 10^{-4}$ mK², (ii) the histogram (red) curve corresponds to the negative pixel's temperatures, (iii) the dashed (violet) line corresponds to the positive pixel's temperatures, and (iv) the triangles represent the distribution of the negative pixels' temperatures corresponding to a modified V map where the cold-spot temperature is 70% of its original value.

given WMAP map (which, at the angular scales we are interested, shall introduce a spurious signal in the next NS-asymmetry analysis) we investigate several X-cases. In fact, we discover that when the cold-spot temperature is 70% of its original value, or lower, the non-linear tail disappears. Consistently, in the 70%-case the skewness is -0.0323, -0.0294, and -0.0334, for the Q, V, and W maps, respectively. In conclusion, the diminution of the cold-spot temperature implies the suppression of the non-linear tail in the temperature distribution plot.

III. SIGMA-MAP METHOD

Now we are interested in studying the effect of these cold-spot temperature changes on the angular-correlation strengths in WMAP maps. For this we use a geometrical-statistical method that leads us to quantify, in intensity and direction, the CMB angular correlations, in particular, to search for an hemispherical asymmetry (for details of this method see Ref. [10]).

Let $\Omega_{\gamma_0}^J \equiv \Omega(\theta_J, \phi_J; \gamma_0) \subset \mathcal{S}^2$ be a spherical cap region on the celestial sphere \mathcal{S}^2 , of γ_0 degrees of aperture, with vertex at the J th pixel, $J = 1, \dots, N_{\text{caps}}$, where (θ_J, ϕ_J) are the angular coordinates of the J th pixel's center. Both the number of spherical caps N_{caps} and the coordinates of their centers (θ_J, ϕ_J) are defined using the HEALPIX pixelization scheme [9]. The union of the N_{caps} spherical caps covers completely \mathcal{S}^2 .

Given a pixelized CMB map, the 2-point angular-correlation function (2PACF) of the temperature fluctuations, $T = T(\theta, \phi)$, corresponding to the pixels located in the spherical cap $\Omega_{\gamma_0}^J$ is defined by $C(\gamma)^J \equiv \langle T(\theta_i, \phi_i)T(\theta_{i'}, \phi_{i'}) \rangle$, where $\cos \gamma = \cos \theta_i \cos \theta_{i'} + \sin \theta_i \sin \theta_{i'} \cos(\phi_i - \phi_{i'})$, and $\gamma \in (0, 2\gamma_0]$ is the angular distance between the i th and the i' th pixels' centers. The average $\langle \rangle$ in the above definition is done over all the products $T(\theta_i, \phi_i)T(\theta_{i'}, \phi_{i'})$ such that $\gamma_k \equiv \gamma \in ((k-1)\delta, k\delta]$, for $k = 1, \dots, N_{\text{bins}}$, where $\delta \equiv 2\gamma_0/N_{\text{bins}}$ is the bin width. We denote by $C_k^J \equiv C(\gamma_k)^J$ the value of the 2PACF for the angular distances $\gamma_k \in ((k-1)\delta, k\delta]$. Now, consider a scalar function $\sigma : \Omega_{\gamma_0}^J \subset \mathcal{S}^2 \mapsto \mathbb{R}^+$, for $J = 1, \dots, N_{\text{caps}}$, which assigns to the J cap, centered at (θ_J, ϕ_J) , a real positive number $\sigma_J \equiv \sigma(\theta_J, \phi_J) \in \mathbb{R}^+$. We define σ_J as

$$\sigma_J^2 \equiv \frac{1}{N_{\text{bins}}} \sum_{k=1}^{N_{\text{bins}}} (C_k^J)^2. \quad (1)$$

To obtain a quantitative measure of the angular correlations in a CMB map, we cover the celestial sphere with N_{caps} spherical caps, and calculate the set of sigma values $\{\sigma_J, J = 1, \dots, N_{\text{caps}}\}$ using Eq. (1). Associating the sigma value σ_J to the J th pixel, for $J = 1, \dots, N_{\text{caps}}$, one fills the celestial sphere with positive real numbers. Then, according to a linear scale (where $\sigma^{\text{min}} \rightarrow \text{blue}$, $\sigma^{\text{max}} \rightarrow \text{red}$), one converts this sigma-values map into a colored map: this is the sigma map. Finally, we find the multipole components of a sigma map $\sigma(\theta, \phi) = \sum_{\ell, m} A_{\ell m} Y_{\ell m}(\theta, \phi)$, and calculate its angular power spectrum $\{S_\ell, \ell = 1, 2, \dots\}$, that is

$$S_\ell \equiv \frac{1}{2\ell + 1} \sum_{m=-\ell}^{\ell} |A_{\ell m}|^2. \quad (2)$$

Accordingly, the power spectrum S_ℓ of a sigma map computed from a WMAP map provides quantitative information of its statistical anisotropy features as compared with the mean of the sigma-map power spectra obtained from simulated isotropic Gaussian CMB maps.

With this aim we produced a set of 1000 Monte Carlo (MC) CMB maps, which correspond to random realizations seeded by the Λ CDM angular power spectra [1], with $\ell = 2 - 512$ ($N_{\text{side}} = 256$). From these full-spectrum MC maps we generate, similarly as we have done with the WMAP data, a set of MC maps containing the multipoles $\ell = 11 - 20$ ($N_{\text{side}} = 32$). We then calculate the sigma maps of these MC maps (hereafter sigma-maps MC) and their corresponding angular power spectra using eq. (2). Last, we compute statistical significance by comparing the power spectra of the sigma-maps WMAP with the spectra from the sigma-maps MC. For these spectra, $S_\ell \simeq 0$, for $\ell \geq 5$, thus we only consider the multipole range $\{S_\ell, \ell = 1, \dots, 5\}$. S_1 corresponds to the dipolar anisotropy strength.

IV. RESULTS AND CONCLUSIONS

As observed in Fig. 2 top's panel, this sigma-map WMAP-V clearly exhibits a dipolar red-blue region indicating a hemispherical asymmetry in the distribution of the angular correlations power, this is the NS-asymmetry anomaly at medium angular scales ($\ell = 11 - 20$). In fact, in the bottom panel of Fig. 2 we show its angular power spectrum and confirm, for the 100%-case, that its dipole term is indeed anomalous, unexpected in 97.6% of the sigma-maps MC for the sigma-map V (97.6% and 97.5% for sigma-map Q and sigma-map W, respectively). Moreover, we studied the effects caused by a systematic reduction of the cold-spot temperature. Our results, for the cases $X = 90, 70, 50, 30$, and 0, shown also in the bottom panel of Fig. 2, illustrate that successively lowering the cold-spot temperature implies the monotonic decrease of the dipole intensity, S_1 , which in turn means the loss of statistical significance of the NS-asymmetry phenomenon. Consistently, the triangles data corresponding to the 70%-case shown in Figs. 1 and 2, illustrate the correlation found here: the weakening of non-Gaussian features in the cold spot implies the fading of the anomalous NS-asymmetry in WMAP maps. A correlation between a non-Gaussian feature (i.e., the cold spot) and a large-scale anisotropy (i.e., the NS-asymmetry) has been established. Another crucial issue concerns the case $X=0$, which corresponds to the absence of the cold spot in CMB maps. For $X=0$ the dipole intensity S_1 decreases 59.6% with respect to the case $X=100$ for the sigma-map V (while it decreases 58.7% and 60.4% for the sigma-map Q and sigma-map W, respectively), achieving a value very close to the mean obtained averaging the sigma-maps-MC spectra. Additionally, we have investigated nine other spots, the coldest and hottest ones in the southern hemisphere of WMAP maps, to know their influence on NS-asymmetry phenomenon. Considering separately the case $X=0$ for these nine spots, our results show that none of them reduces the confidence level of the hemispherical asymmetry below 90% C.L. In conclusion, the (non-Gaussian) cold spot is responsible for 60% of the anoma-

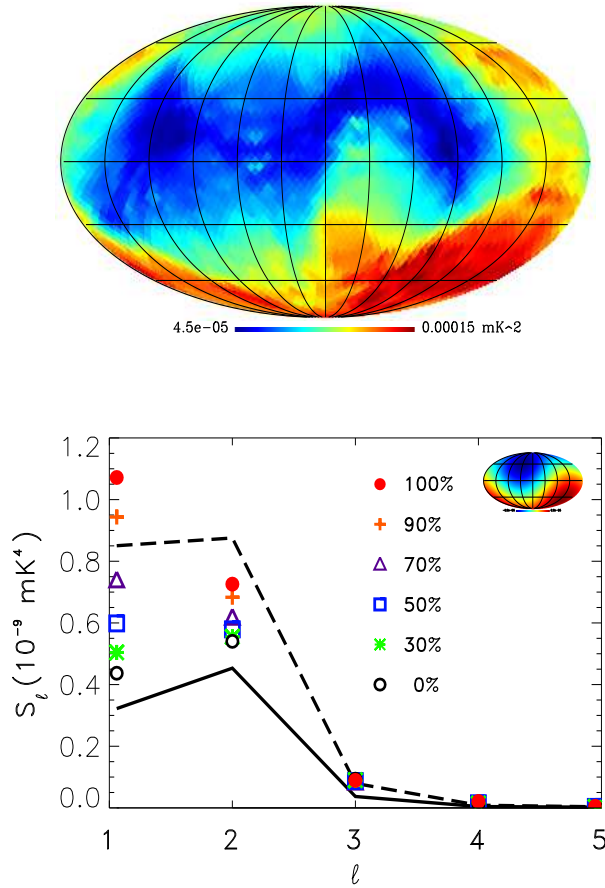


FIG. 2: Top: This is the sigma-map WMAP-V obtained using $\gamma_0 = 45^\circ$, $N_{\text{bins}} = 45$, and $N_{\text{caps}} = 3072$. The NS-asymmetry phenomenon is clearly seen in the uneven hemispherical distribution of the angular correlation's strengths, depicted as red and blue pixels (large and small σ_J , respectively). Bottom: Angular power spectra of the sigma map shown above (100%-case) and sigma maps from several cases: X = 90, 70, 50, 30, and 0, where the cold-spot temperature in the V map is a fraction, X%, of its original value. The solid (dashed) line corresponds to the mean (95.4% CL) spectra of 1000 sigma-maps MC. The statistical significance of the NS-asymmetry is revealed at 97.6% CL in the 100%-case, while for the 70%-case it is 91.5% CL. The dipole component of the above sigma map, displayed in the inset, points toward $(l, b) \simeq (225^\circ, -45^\circ)$.

lous NS-asymmetry power observed in WMAP data, at medium angular scales.

It is well known [1] that CMB foregrounds are frequency dependent. For this, in order to find out possible foreground signatures in our findings we used the Q, V, and W band maps. In fact, robustness tests (see Table I) and sigma-map outcomes studying these three maps are not significantly different, meaning that our results are unlikely due to residual foregrounds. Pixel

TABLE I: Robustness tests for sigma-map analyses using several parameters. Here are the confidence levels (CL) for S_1 in the NS-asymmetry analyses in Q, V, and W maps ($N_{\text{side}} = 32$, pixel size $1.8^\circ \Rightarrow \delta \equiv 2\gamma_0/N_{\text{bins}} \gtrsim 2^\circ$). The C.L. intervals correspond to different binning tests: $N_{\text{bins}} = 15, 30, 45, 60$, provided $\gamma_0 \geq N_{\text{bins}}$ to minimize the statistical noise in σ_J calculations.

maps \ (Ncaps, γ_0)	(768,30°)	(768,45°)	(3072,45°)	(768,60°)
Q	94%–96%	97%–98%	97%–98%	94%–96%
V	94%–96%	97%–98%	97%–98%	94%–96%
W	94%–96%	97%–98%	97%–98%	94%–96%

noise in WMAP maps is another possible source of incorrect results. However, at the angular scales we are working, pixel noise artifact is dominated by the cosmic variance [1], and this effect was already included in Monte Carlo maps. In fact, pixel noise in WMAP data for $\ell = 11 - 20$ is of the order $1\mu\text{K}$, while temperature uncertainty due to cosmic variance is $\sim 5\mu\text{K}$. Consequently, the robustness of our analyses supports the validity of our NS-asymmetry results.

There is strong evidence for NS-asymmetry at several angular scales in WMAP data [2]. In addition, we know that different angular scales in the CMB field encode information corresponding to distinct physical phenomena. Therefore, it is highly plausible that NS-asymmetry at different scales has not a common origin. One manifestation of this is the fact that the dipolar direction of hemispherical asymmetry is distinct for large ($\ell = 2 - 10$) and medium ($\ell = 11 - 20$) angular scales, i.e., $\sim (220^\circ, -20^\circ)$ [2] and $\sim (225^\circ, -45^\circ)$, respectively. Here we focused on those angular scales compatible with cold-spot dimensions, that is $\theta \simeq 9^\circ - 16^\circ$ [3] (i.e., $\ell = 11 - 20$, where $\ell \sim \pi/\theta$). Clearly, the effect of the cold spot does not start at $\ell = 11$ neither does it end at $\ell = 20$. For $\ell \leq 10$ the cold-spot influence contends with colder and hotter spots, this is because the angular power spectra $C_\ell \propto 1/(\ell(\ell + 1))$ (Sachs-Wolfe effect) is larger for smaller ℓ , and seems difficult to cause the NS-asymmetry at large-angles. On the other hand, the impact of the cold spot on NS-asymmetry for smaller scales, $\ell \geq 21$, is unknown and deserves further investigation. These facts lead us to conclude that it might be possible that distinct phenomena are causing the reported hemispherical asymmetry at several angular scales [2], and what is really happening is that different phenomena are predominant at distinct angular scales. Of course, the origin of the cold spot, including the possibility that it is just an anomalous statistical fluke, is still an open question.

Acknowledgements

We thank A. F. F. Teixeira, M. J. Rebouças, and G. D. Starkman for critical reading and suggestions. This work was supported by CNPq (309388/2008-2). We are

grateful for the use of the Legacy Archive for Microwave Background Data Analysis (LAMBDA) [1]. Some of the

results in this paper have been derived using the HEALPIX package [9].

-
- [1] C. L. Bennett *et al.*, *Astrophys. J. Suppl. Ser.* **148**, 1 (2003); G. Hinshaw *et al.*, *Astrophys. J. Suppl. Ser.* **170**, 288 (2007); G. Hinshaw *et al.*, *Astrophys. J. Suppl. Ser.* **180**, 225 (2009).
- [2] F. K. Hansen, A. J. Banday, and K. M. Górski, *Mon. Not. R. Astron. Soc.* **354**, 641 (2004); H. K. Eriksen *et al.*, *Astrophys. J.* **605**, 14 (2004); K. Land and J. Magueijo, *Phys. Rev. Lett.* **95**, 071301 (2005); C. J. Copi *et al.*, *Mon. Not. R. Astron. Soc.* **367**, 79 (2006); A. Bernui *et al.*, *Astron. Astrophys.* **454**, 409 (2006); Y. Wiaux, P. Vielva, E. Martínez-González, and P. Vandergheynst, *Phys. Rev. Lett.* **96**, 151303 (2006); L. R. Abramo, A. Bernui, I. S. Ferreira, T. Villela, and C. A. Wuensche, *Phys. Rev. D* **74**, 063506 (2006); C. J. Copi, D. Huterer, D. J. Schwarz, and G. D. Starkman, *Phys. Rev. D* **75**, 023507 (2007); D. Huterer, *New Astron. Rev.* **50**, 868 (2006); K. Land and J. Magueijo, *Mon. Not. R. Astron. Soc.* **378**, 153 (2007); A. Bernui *et al.*, *Astron. Astrophys.* **464**, 479 (2007); P. K. Samal *et al.*, arXiv:0708.2816 [astro-ph]; P. K. Samal *et al.*, *Mon. Not. R. Astron. Soc.* **396**, 511 (2009); B. Lew, *JCAP* 0808:017 (2008); B. Lew, *JCAP* 0809:023 (2008); A. Bernui and W. S. Hipólito-Ricaldi, *Mon. Not. R. Astron. Soc.* **389**, 1453 (2008); F. K. Hansen *et al.*, arXiv:0812.3795 [astro-ph]; J. Hoftuft *et al.*, *Astrophys. J.* **699**, 985 (2009); Y. Ayaita, M. Weber, and C. Wetterich, arXiv:0905.3324 [astro-ph]; M. Frommert and T. A. Ensslin, arXiv:0908.0453 [astro-ph]; C. Dickinson *et al.*, arXiv:0903.4311 [astro-ph]; L. R. Abramo, A. Bernui, and T. S. Pereira, arXiv:0909.5395 [astro-ph].
- [3] P. Vielva *et al.*, *Astrophys. J.* **609**, 22 (2004); M. Cruz *et al.*, *Mon. Not. R. Astron. Soc.* **356**, 29 (2005); M. Cruz *et al.*, *Mon. Not. R. Astron. Soc.* **369**, 57 (2006); P. Vielva *et al.*, *Mon. Not. R. Astron. Soc.* **381**, 932 (2007); Y. Wiaux *et al.*, *Mon. Not. R. Astron. Soc.* **385**, 939 (2008); J. D. McEwen *et al.*, *Mon. Not. R. Astron. Soc.* **388**, 659 (2008); P. Naselsky *et al.*, arXiv:0712.1118 [astro-ph]; D. Pietrobon *et al.*, *Phys. Rev. D* **78**, 103504 (2008); M. Cruz, E. Martínez-González and P. Vielva, arXiv:0901.1986 [astro-ph]. D. Pietrobon *et al.*, arXiv:0905.3702 [astro-ph]; G. Rossmanith *et al.*, arXiv:0905.2854 [astro-ph].
- [4] P. D. Naselsky, L.-Y. Chiang, P. Olesen, and I. Novikov, *Phys. Rev. D* **72** (2005) 063512; A. de Oliveira-Costa and M. Tegmark, *Phys. Rev. D* **74**, 023005 (2006); A. Gruppuso and C. Burigana, *JCAP* 0908:004 (2009). P. Bielewicz *et al.*, *Astrophys. J.* **635**, 750 (2005); A. Bernui *et al.*, *Int. Journal of Mod. Phys. D* **16**, 411 (2007); P. Vielva and J. L. Sanz, *Mon. Not. R. Astron. Soc.* **397**, 837 (2009); M. Kawasaki *et al.*, *JCAP* 0901:042 (2009); A. Bernui and M. J. Rebouças, *Phys. Rev. D* **79**, 063528 (2009); D. J. Schwarz, G. D. Starkman, D. Huterer, and C. J. Copi, *Phys. Rev. Lett.* **93**, 221301 (2004); E. F. Bunn, *Phys. Rev. D* **75**, 083517 (2007);
- [5] C. Gordon, W. Hu, D. Huterer, and T. Crawford, *Phys. Rev. D* **72**, 103002 (2005); L. Ackerman, S. M. Carroll, and M. B. Wise, *Phys. Rev. D* **75**, 083502 (2007); T. S. Pereira, C. Pitrou, and J.-P. Uzan, *JCAP* 0709:006 (2007); C. Pitrou, T. S. Pereira, and J.-P. Uzan, *JCAP* 0804:004 (2008); T. S. Pereira and L. R. Abramo, *Phys. Rev. D* **80**, 063525 (2009); L. Campanelli, P. Cea, and L. Tedesco, *Phys. Rev. Lett.* **97**, 131302 (2006); L. Campanelli, P. Cea, and L. Tedesco, *Phys. Rev. D* **76**, 063007 (2007); L. Campanelli, *Phys. Rev. D*, **80**, 063006 (2009); A. L. Erickcek, M. Kamionkowski, and S. M. Carroll, *Phys. Rev. D* **78**, 123520 (2008); Y. Shtanov and H. Pyatkovska, *Phys. Rev. D* **80**, 023521 (2009); I. Y. Areféva, N. V. Bulatov, L. V. Joukovskaya, and S. Y. Vernov, arXiv:0903.5264 [hep-th]; C. M. Hirata, *JCAP* 0909:011 (2009); T. Kahniashvili, G. Lavrelashvili, and B. Ratra, *Phys. Rev. D* **78**, 063012 (2008); T. R. Seshadri and K. Subramanian, *Phys. Rev. Lett.* **103**, 081303 (2009); C. Caprini, F. Finelli, D. Paoletti, and A. Riotto, *JCAP* 0906:021 (2009); J. Kim and P. Naselsky, *JCAP* 0907:041 (2009).
- [6] A. Rakić and D. J. Schwarz, *Phys. Rev. D* **75**, 103002 (2007).
- [7] A. Bernui, *Phys. Rev. D* **78**, 063531 (2008).
- [8] D. Pietrobon, arXiv:0907.4443 [astro-ph].
- [9] K. M. Górski *et al.*, *Astrophys. J.* **622**, 759 (2005).
- [10] A. Bernui, I. S. Ferreira, and C. A. Wuensche, *Astrophys. J.* **673**, 968 (2008).